Peer Reviewed Article openaccess

Hyperspectral reflectance for non-invasive early detection of black shank disease in flue-cured tobacco

Austin Hayes* and T. David Reed

Virginia Polytechnic Institute and State University, USA and Southern Piedmont Agricultural Research and Extension Center, Blackstone, VA, USA

Contacts
Austin Hayes: Austin.Hayes.Contractor@altria.com David Reed: threed@vt.edu
https://orcid.org/0000-0001-5888-3764

Flue-cured tobacco (*Nicotiana tabacum* L.) is a high value-per-acre crop that is intensively managed to optimise the yield of high-quality cured leaf. A 15-day study assessed the potential of hyperspectral reflectance data for detecting *Phytophthora nicotianae* (black shank) incidence in flue-cured tobacco. Hyperspectral reflectance data were taken from a commercial flue-cured tobacco field with a progressing black shank infestation. The effort encompassed two key objectives. First, develop hyperspectral indices and/or machine learning classification models capable of detecting *Phytophthora nicotianae* (black shank) incidence in flue-cured tobacco. Second, evaluate the model's ability to separate pre-symptomatic plants from healthy plants. Two hyperspectral indices were developed to detect black shank incidence based on differences in the spectral profiles of asymptomatic flue-cured tobacco plants compared to those with black shank symptoms. While one of the indices is a broad-band index and the other uses narrow wavelength values, the statistical difference between the two indices was not significant and both provided an accurate classification of symptomatic plants. Further analysis of the indices showed significant differences between the index values of healthy and symptomatic plants ($\alpha = 0.05$). In addition, the indices were able to detect black shank symptoms pre-symptomatically ($\alpha = 0.09$). Subspace linear discriminant analysis, a machine learning classification, was also used for prediction of black shank incidence with up to 85.7% classification accuracy. The implications of using either spectral indices or machine learning for classification for future black shank research are discussed.

Introduction

Phytophthora nicotianae (black shank) is a soilborne fungus-like pathogen of tobacco. Common symptoms are chlorosis, wilting of the leaves, stalk rot and eventual plant death.[1] Black shank is one of the most common and detrimental pathogens of flue-cured tobacco crops in Virginia. If left untreated, black shank infestations can cause 100% loss in some fields.[1] The research presented here investigates the potential for development of an early detection system for black shank using point spectroscopy, in the field. The purpose of the research is to facilitate future analysis of hyperspectral imagery collected by unmanned aerial vehicle (UAV).

The sensor(s) carried by a UAV determine(s) the data type and quality measured. Hyperspectral sensors have a higher spectral resolution than multispectral sensors and measure hundreds of very narrow bands ranging

Correspondence
Austin Hayes (Austin.Hayes.Contractor@altria.com)

Received: 13 April 2021
Revised: 7 July 2021
Accepted: 12 July 2021
Publication: 28 September 2021
doi: 10.1255/jsi.2021.a4
ISSN: 2040-4565

Citation
A. Hayes and T.D. Reed, "Hyperspectral reflectance for non-invasive early detection of black shank disease in flue-cured tobacco", *J. Spectral Imaging* **10,** a4 (2021). https://doi.org/10.1255/jsi.2021.a4

from 1 nm to 30 nm wide on the electromagnetic spectrum. Hyperspectral cameras store data as a 3-D matrix, with the x and y planes consisting of pixels representing the target surface (like a normal image) and the z plane consisting of a stack of those images, each representing a narrow wavelength range.[2] Point spectroscopy sensors, such as the spectroradiometer used in this study, could be equated to one pixel of a hyperspectral image. These sensors render a spectral profile, or spectral signature, of a target surface with the electromagnetic spectrum as the x-axis and electromagnetic energy on the y-axis.[3]

Hyperspectral imagery is better suited to predicting specific plant properties, when compared to multispectral imaging,[4] and is a promising technology for plant phenotyping.[5] Hyperspectral imaging has been proven effective for detecting tobacco mosaic virus (TMV) pre-symptomatically.[6] In other crops, ground-based hyperspectral data have been used to detect specific disease incidence of tomato spotted wilt virus (TSWV) in capsicum plants,[7] peanut leaf spot in peanuts,[8] yellow leaf curl in tomatoes[9] and charcoal rot disease in soybeans.[10] Hyperspectral data have the potential to be a powerful tool for disease detection of plants[11] by allowing us to quantify physiological changes in a broad range of crops.[12]

Black shank infestations cause major physiological changes to flue-cured tobacco plants. The pathogen damages the roots of the plant, which impacts water and nutrient uptake.[1] This reduction in the plants' ability to access crop inputs leads to wilting and chlorosis, or yellowing, of the leaves. The hypothesis is that this change in leaf physiology can be measured using point spectroscopy. Therefore, a field study was conducted in a commercial field with a black shank infestation to evaluate the use of hyperspectral data to detect black shank incidence in flue-cured tobacco. The objectives of this study were:

1) Observe differences in the mean spectral profiles of black shank symptomatic plants and asymptomatic plants.
2) Investigate the potential of developing a hyperspectral index to detect black shank incidence before quality and yield is significantly reduced.
3) Determine specificity of the hyperspectral index to black shank detection by testing the proposed index on *Ralstonia solanacearum* (Granville wilt) symptomatic and asymptomatic plants.
4) Test the ability of machine learning algorithms to predict symptomatic and asymptomatic plants and compare the accuracy of machine learning algorithms to the proposed hyperspectral index.

Materials and methods

Data acquisition

A commercial flue-cured tobacco production field near Union Level, VA, USA with a quickly spreading black shank infestation was observed during the 2018 growing season. An observation area of 40 consecutive plants was selected. The area was chosen because of the equal distribution of black shank symptoms in the area. At the inception of the experiment, approximately half of the plants in the observation area displayed varying levels of disease symptoms and half appeared healthy.

Reflectance spectra were measured using an SR-3500 (Spectral Evolution, Lawrence, MA) full range (350–2500 nm) spectroradiometer. The spectral resolution of the SR-3500 is 3 nm at 700 nm, 8 nm at 1500 nm and 6 nm at 2100 nm. The spectroradiometer was used with a leaf-clip attachment in order to minimise atmospheric effects (Figure 1). A piece of 99 % diffuse reflectance material was used to radiometrically correct the spectra during data acquisition, and the spectroradiometer stored the data in terms of true reflectance. This reflectance data was used for analysis with no additional preprocessing. Measurements of each plant in the observation area were taken on four dates: 2, 9, 13 and 17 August. This was after terminal inflorescence had been removed and directly prior to harvest. Measurements were taken from the third leaf from the top of each plant between the sixth and seventh lateral vein from the base of the leaf. At all observation dates, a visual health rating was recorded as asymptomatic, symptomatic or diseased for each plant in the observation area (Figure 2). Plants rated as asymptomatic exhibited no visual disease symptoms. Symptomatic plants had early visual symptoms of black shank, such as yellowing and wilting of lower leaves. Diseased-rated plants had developed significant black shank symptoms, including severe wilting, necrosis and stalk rot. Table 1 shows the number of plants rated in each group on each observation date.

A follow-up field study was conducted in a *Ralstonia solanacearum* (Granville wilt) infested flue-cured tobacco production field near Kenbridge, VA. The same equipment was used as that in the black shank study. The protocol was the same except that the number of plants measured was 20. Health ratings used were asymptomatic, symptomatic and diseased. The objective was to examine the mean spectral profiles of black shank and Granville wilt infected plants to evaluate whether a hyperspectral index developed to detect black shank symptoms would be specific to black shank, given that

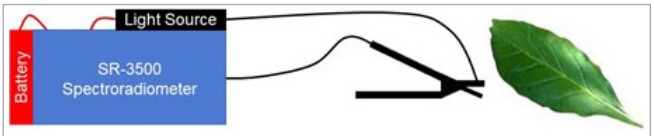

Figure 1. Diagram of SR-3500 with leaf clip attachment. A fibre optic cable carries light from the light source to the leaf clip stage and a data cable runs from the spectroradiometer to the leaf clip. The red lines represent power cables that supply the spectroradiometer and the light source.

Figure 2. Representative plants of each plant health rating for the black shank study conducted near Union Level, VA in 2018.

Table 1. Number of plants in each rating group for all observation dates of the black shank study conducted in Union Level, VA.

	Observation date			
	2 August	9 August	13 August	17 August
Asymptomatic	25	8	8	8
Symptomatic	11	18	18	12
Diseased/dead	4	14	14	20

Granville wilt symptoms can often look like that of black shank.[1] Data was collected on 2, 11 and 18 September 2018. This was after the removal of terminal inflorescence and directly prior to final harvest.

Data analysis

Mean spectral profiles were calculated for each health rating on each observation date and plotted using SigmaPlot 12.3 (Systat Software, Inc., San Jose, CA). Reflection values at each wavelength within the mean spectral profiles were investigated statistically using PROC T-test in SAS statistical software (SAS Institute, Cary, NC) and indices were developed based on these differences. Differences in index values between asymptomatic and symptomatic plants were evaluated using analysis of variance (ANOVA). In order to assess the ability to detect black shank incidence pre-symptomatically, two new separate groups of spectral profiles from the 2 August dataset were organised to conduct a pre-symptomatic test. The healthy group consisted of all the plants that were rated asymptomatic on 2 and 9 August and the pre-symptomatic group contained plants that were rated asymptomatic on 2 August but rated symptomatic on 9 August. Mean spectral profiles of the pre-symptomatic detection groups were plotted and the index values were statistically analysed using ANOVA.

The symptomatic and pre-symptomatic data sets were used to train supervised machine learning classification algorithms in Matlab (MathWorks, Inc., Natick, MA). Supervised machine learning algorithms use predictor variables (in this case health ratings) and a set of response variables (reflectance values) to train a model to make predictions about new data. A total of 22 supervised machine learning algorithms were trained with the data and subspace linear discriminant analysis (LDA) was chosen as the model with the best accuracy. Subspace LDA is a machine learning algorithm that uses principal component analysis (PCA) as a preprocessor to reduce the dimensionality of the data before using LDA to find a linear transformation which minimises the scatter within groups and maximises the scatter between groups.[13] A key output of subspace LDA is the confusion matrix (Figure 3), which is designed to display the amount of correct and incorrect predictions for each group and allow for calculation of performance statistics for a given model.[14]

Quadrant 1 shows the number of true symptomatic predictions. In this study, the true symptomatic predictions are the measurements which were visually rated symptomatic and correctly classified as symptomatic by subspace LDA. False symptomatic predictions, in quadrant 2, are measurements that were visually rated symptomatic but incorrectly classified as asymptomatic. False asymptomatic predictions, in quadrant 3, are measurements that were visually rated asymptomatic but classified as symptomatic. Quadrant 4 contains the number of true asymptomatic predictions, those measurements that were visually rated asymptomatic and correctly classified as asymptomatic by subspace

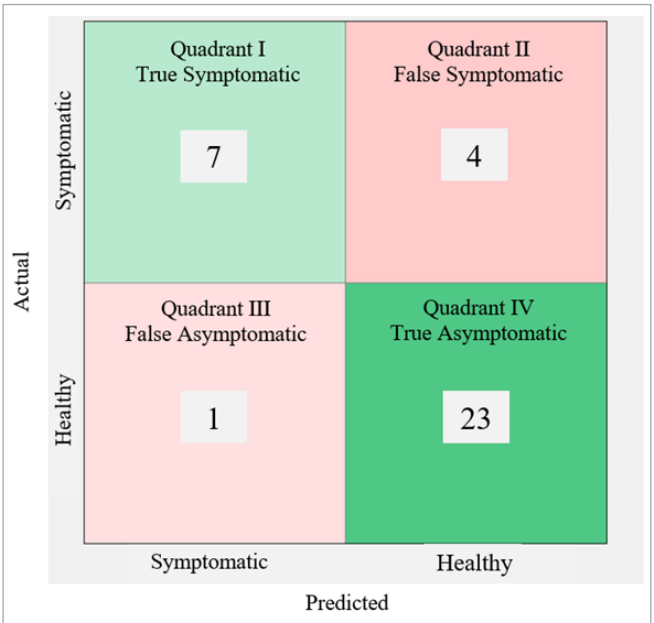

Figure 3. Example of a confusion matrix used to analyse subspace LDA performance. Quadrant I and IV show correct predictions based on plant health counts.

LDA. Darker shades of red or green in each quadrant of the confusion matrix indicate increasing prediction values for that quadrant. An important measure of a supervised classification's performance is classification accuracy. Classification accuracy is defined as the number of true predictions divided by the total number of predictions times 100. Precision, recall and F1 score are three additional performance measures used for analysing the strength and accuracy of a supervised classification model. Precision is the number of true symptomatic predictions divided by the number of true symptomatic predictions and false symptomatic predictions, and a low precision value indicates a large number of false symptomatic predictions in relation to true symptomatic predictions. In this case, a low precision value would mean the model did not classify symptomatic plants accurately. Recall is the number of true symptomatic predictions divided by the number of true symptomatic predictions and false asymptomatic predictions. A low recall means there is a large number of false asymptomatic predictions in relation to true symptomatic predictions. The F1 score is a statistic that measures the balance between precision and recall. A low F1 score indicates unbalance between the two. The formula is given below.

$$\text{F1 Score} = 2 \times \frac{precision \times recall}{precision + recall}$$

Results and discussion

Evaluation of mean spectral profiles

Mean spectral profiles from the first observation date of the black shank study showed differences in the disease rating groups (Figure 4). The reflectance in the visible range (550–675 nm) increased with disease symptom expression. In the near infrared (NIR) range (700–1500 nm), the reflectance of the heathy plants was lower than that of the symptomatic and diseased group. However, the symptomatic group had the highest reflectance. Reflectance in the short-wave infrared (SWIR) range (1500–2500 nm) followed the same trends seen from 550 nm to 675 nm.

The diseased group was comprised of severely infected plants and exhibited the same spectral characteristics as the symptomatic group, only with more pronounced increases in reflectance, compared to the mean spectral profiles of the asymptomatic plants on the first observation date (Figure 4). Detecting black shank incidence as soon as possible was important. Therefore, only the asymptomatic and symptomatic groups were analysed further. The reflectance in the SWIR (1500–2500 nm) followed similar trends as reflectance in the visual range. Sensors and cameras that measure only in the visual and NIR range are considerably less expensive than those that measure SWIR reflectance. There is value in making any proposed index relevant to future research and industry uses at the lowest possible cost. For these reasons, the spectral range that was chosen for index development was 350–1500 nm, or the visible and NIR range.

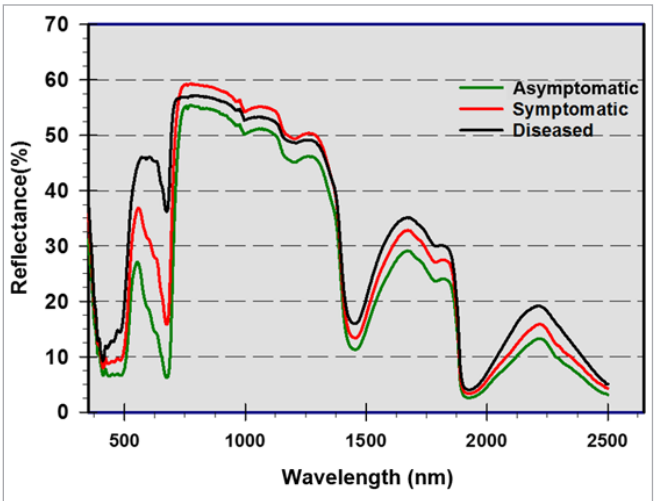

Figure 4. Mean spectral profiles of three disease rating groups in the black shank study conducted near Union Level, VA in 2018 at the first observation date (2 August).

The mean spectral profiles of the asymptomatic and symptomatic groups for each observation date are shown in Figure 5. As disease development and symptom expression continued to progress, individual plants would be reclassified from the asymptomatic group to the symptomatic group if visual symptoms were observed and plants that were reclassified from the symptomatic group to the diseased group were removed from the analysis. On each date, the mean spectral profiles represent plants rated asymptomatic or symptomatic on that specific observation date. Thus, in the visible range of the spectrum, the reflectance of each group stayed consistent throughout the study. The difference in reflectance between the spectral profiles of the asymptomatic and symptomatic groups, for all four observation dates, from 550 nm to 675 nm was significant ($p < 0.001$). The reflectance in the NIR was less consistent and there were no significant differences between the groups. The NIR reflectance was higher for the symptomatic plants on 2 and 17 August, similar on 9 August and lower on 13 August when compared to the asymptomatic plants.

The mean spectral profiles of the healthy and pre-symptomatic groups on 2 August (Figure 6) show similar differences to those shown between asymptomatic and symptomatic groups. Pre-symptomatic plants were those that were reclassified as symptomatic at the following assessment. In the 550–675 nm range, the pre-symptomatic plants had a higher mean reflectance compared to healthy plants. The difference in reflectance over this range was not as large as seen in the

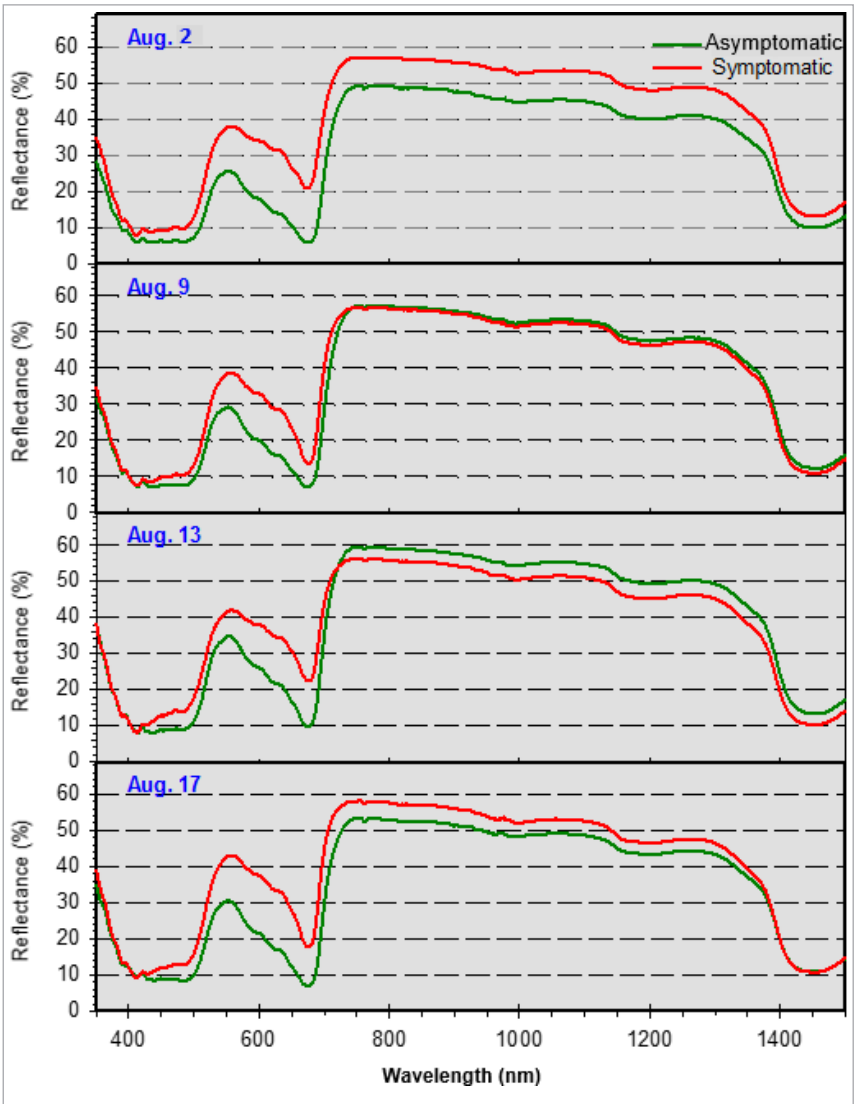

Figure 5. Mean spectral profiles of the black shank asymptomatic and symptomatic groups for all four observation dates of the 2018 black shank study conducted near Union Level, VA.

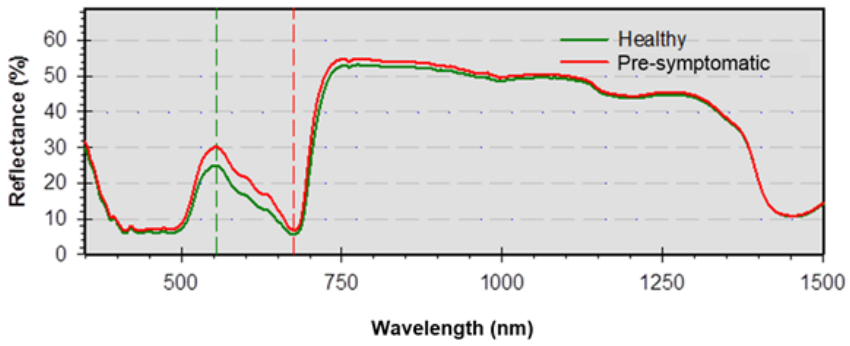

Figure 6. Mean spectral profiles of the two pre-symptomatic black shank detection groups. The data for the pre-symptomatic test was taken on the first observation date of the study (2 August).

mean spectral profiles of asymptomatic and symptomatic plants. The differences in NIR reflectance between the pre-symptomatic plants and healthy plants were not significantly different.

Definition and assessment of proposed indices

Two black shank detection indices were developed based on the differences in the mean spectral profiles between the symptomatic and asymptomatic groups. The first was a broad-band index with reflectance values averaged over broad ranges of the spectrum and the second was a narrow-band index with two distinct wavelength reflectance values. Values for both indices range from 0 to 1, with increasing values indicating increased probability of black shank incidence. The formulas for which are given below, where r_x equals reflectance (r) at wavelength in nm (x).

Broad - band Black Shank Index	**Narrow - band Black Shank Index**
$\frac{\text{Avg}(r_{550} - r_{675})}{\text{Avg}(r_{750} - r_{1200})}$	$\frac{r_{675}}{r_{800}}$

The significant differences in the 550–675 nm range ($p < 0.0001$) and the lack of significant differences in the 750–1200 nm range, with respect to black shank symptoms, were the justification for wavelength selection for the numerator and denominator of both indices. The numerator of the equation is related to changes in reflectance based on disease incidence, while the denominator is used as a normalising factor.

The differences between the broad-band black shank index values for the asymptomatic and symptomatic group were significant for the first three observation dates ($\alpha = 0.05$) and significant on the fourth observation date at $p = 0.0754$ (Table 2). For the narrow-band black shank index, the first three observation dates were also statistically significant ($\alpha = 0.05$) with the fourth date being significant at $p = 0.0548$ (Table 3). The index values for the pre-symptomatic comparison had lower p-values than seen in the symptomatic comparison. However, for the pre-symptomatic comparison, the difference in the groups for the broad-band and narrow-band index were significant at $p = 0.0640$ and $p = 0.0860$, respectively. The index values of both the asymptomatic and symptomatic groups increased over time using both indices, possibly due to increased ripening of the crop as well as increasing disease distribution and severity. Both indices performed similarly, with little variation in mean group values or significance between groups. The two indices had a high correlation between them ($r = 0.99$). The high amount of correlation between the broad-band and narrow-band black shank indices indicates that high spectral resolution, such as that of hyperspectral data, is not necessary for classification of black shank incidence. The broad-band black shank index may require a custom multispectral lens for application, since it is calculated using distinct wavelength ranges. However, multispectral cameras are considerably less expensive than hyperspectral cameras available. This cost saving may make the broad-band index more practical and efficient for flue-cured tobacco growers and researchers.

If these indices were to be used with hyperspectral imagery to construct a precision management strategy, an index threshold classification could be performed on the hyperspectral image matrix to render a single-band image that is predictive of black shank distribution within the field. If used in combination with aerial imagery, these indices may provide growers with a rapid and non-invasive

Table 2. Mean broad-band index values for asymptomatic and symptomatic groups, and the pre-symptomatic test grouping for pre-symptomatic plants healthy plants. The *p*-value indicates the significance of difference between the groups for each observation (paired T-test).

	Observation date				
	Pre-symptomatic	Symptomatic			
	2 August	2 August	9 August	13 August	17 August
Mean asymptomatic index value	0.2903	0.3193	0.3646	0.4462	0.4929
Mean symptomatic index value	0.3644	0.5026	0.5330	0.6940	0.6204
p-value	*0.0640*	*0.0007*	*0.0008*	*0.0012*	*0.0754*

Table 3. Mean narrow-band index values for asymptomatic and symptomatic groups, and the pre-symptomatic test grouping for pre-symptomatic plants healthy plants. The *p*-value indicates the significance of difference between the groups for each observation (paired t-test).

	Observation date				
	Pre-symptomatic	Symptomatic			
	2 August	2 August	9 August	13 August	17 August
Mean asymptomatic index value	0.2333	0.2605	0.3062	0.3899	0.4269
Mean symptomatic index value	0.3008	0.4643	0.4820	0.6420	0.5650
p-value	*0.0860*	*0.0004*	*0.0007*	*0.0015*	*0.0548*

tool for scouting for black shank occurrence. It may also be beneficial for assessing the severity and spatial distribution of an active black shank infestation.

Classification using subspace LDA

Index application coupled with threshold classification is one way to classify spectral data for features such as black shank incidence. Another method to classify spectral data is by using machine learning classification algorithms, such as subspace LDA. The performance measures of subspace LDA for symptomatic detection on all four observation dates, as well as the 2 August pre-symptomatic data set, is shown in Table 4. These values were calculated using the confusion matrix for each data set. Classification accuracy was highest on the first observation date. However, all of the other observation dates in the symptomatic test, as well as the pre-symptomatic test, had a higher level of precision. That is, disease detections predicted by subspace LDA for the later observation dates turned out to be more frequently true. Precision is an important measure for any model used to make decisions about where to treat or not treat for black shank. The consequences of treating plants unnecessarily (false asymptomatic) adds to the cost of production, but failing to treat when needed (false symptomatic) will result in decreased yield and quality loss to disease. The first observation date had a high classification accuracy and recall, which exhibits accuracy in correctly predicting plants that were visually rated as heathy. However, a relatively high number of false symptomatic predictions caused the model to have low precision, making this model less desirable. Although the second and third observation dates had a lower classification accuracy, the precision of these models was higher than the first observation date due to a higher percentage of symptomatic plants that were correctly predicted. The fourth observation date had a higher precision value than the first and also had the highest F1 score of the symptomatic comparison. The increased precision values for the last three observation dates may be due to the number of symptomatic plants, relative to asymptomatic plants, included in each dataset (Table 1). The black shank infestation spread, causing more plants to be rated as symptomatic and less plants to be rated asymptomatic as the observation period progressed. The pre-symptomatic model also had good results. A low number of false positives contributed to a high precision value. The model also had a relatively low number of false negatives which bolstered the classification accuracy and recall value.

These results show that there is potential for machine learning algorithms, specifically subspace LDA, to be used in conjunction with hyperspectral cameras to predict symptomatic and pre-symptomatic black shank infestations in flue-cured tobacco in real-time. The advantage

Table 4. Performance measures for subspace LDA trained in Matlab for all observation dates, and the pre-symptomatic test, of the 2018 black shank study conducted near Union Level, VA.

	Observation date				
	2 August	9 August	13 August	17 August	2 August (pre-symptomatic)
Classification accuracy	85.7%	61.5%	69.2%	75.0%	78.3%
Precision	0.64	0.72	0.78	0.77	0.81
Recall	*0.88*	*0.72*	*0.78*	*0.83*	*0.87*
F1 score	*0.74*	*0.72*	*0.78*	*0.80*	*0.84*

of using machine learning, over index threshold-derived maps, is the increased ability of machine learning to be automated. Index threshold-derived maps will need user control to set threshold values, in most cases. However, the ability of the user to set a custom threshold is, in some ways, an advantage of index threshold-derived maps as a means to detect and manage black shank incidence. A particular machine learning model may not work in every situation and provides the user little control over precision. Conversely, index thresholds can be used dynamically by allowing the user to set different thresholds for each unique situation. By setting a conservative (low) threshold, the user can minimise the number of false symptomatic predicted plants. If used for a variable rate fungicide application, this may result in a number of healthy plants being treated. However, a minimal amount of symptomatic and pre-symptomatic plants would be left untreated.

Analysis of tobacco spectral response to Granville wilt

The mean spectral profiles of plants in a Granville wilt infested field are displayed in Figure 7. These data were taken using the same protocol as used in the black shank study. The purpose of this companion study was to investigate the spectral profiles of Granville wilt infested plants to determine if a proposed index or model to detect black shank incidence would be specific to black shank or relevant to a range of tobacco pathogens. The first observation date shows some of the same differences in mean spectral profile of asymptomatic and Granville wilt symptomatic plants shown by the black shank groups. Notably, an increased reflectance from 550 nm to 675 nm for the symptomatic plants. The second and third observation dates do not show any substantial difference in this range. The data suggest that the indices presented to detect black shank incidence would not be useful for detecting Granville wilt incidence. The difference in spectral response of Granville wilt infested plants, compared to that of plants infested with black shank, may be due to the fact that Granville wilt infested plants tend to exhibit less yellowing during disease progression than plants that are infested with black shank, which yellow rather rapidly.

Conclusions

Significant differences in the mean index values of black shank symptomatic plants and asymptomatic plants demonstrated the ability of hyperspectral data to facilitate identification of black shank incidence. The differences in the pre-symptomatic test were significant ($\alpha = 0.10$) for both indices. One would not expect the differences in the mean index values of the pre-symptomatic groups to be as large as that of the symptomatic groups. While the plants in the symptomatic group were visually different and separable from healthy plants, the plants in pre-symptomatic groups were not. Subspace LDA performed relatively well with both the symptomatic and pre-symptomatic groups. Further research is needed to improve the classification accuracy of the model and evaluate the real-time predicting power of subspace LDA, when trained to detect black shank incidence.

This study evaluated the potential for point spectroscopy to detect black shank incidence in flue-cured tobacco. The next step would be to apply the proposed indices to aerial hyperspectral imagery and generate an index threshold-derived map in order to test the ability of the indices to detect black shank incidence at scale. If successful, an index threshold-derived map could be useful for facilitating variable rate fungicide applications as well as predicting the spatial distribution of the pathogen. The ability for hyperspectral data to detect pre-symptomatic black shank incidence exhibits the potential that this technology may have

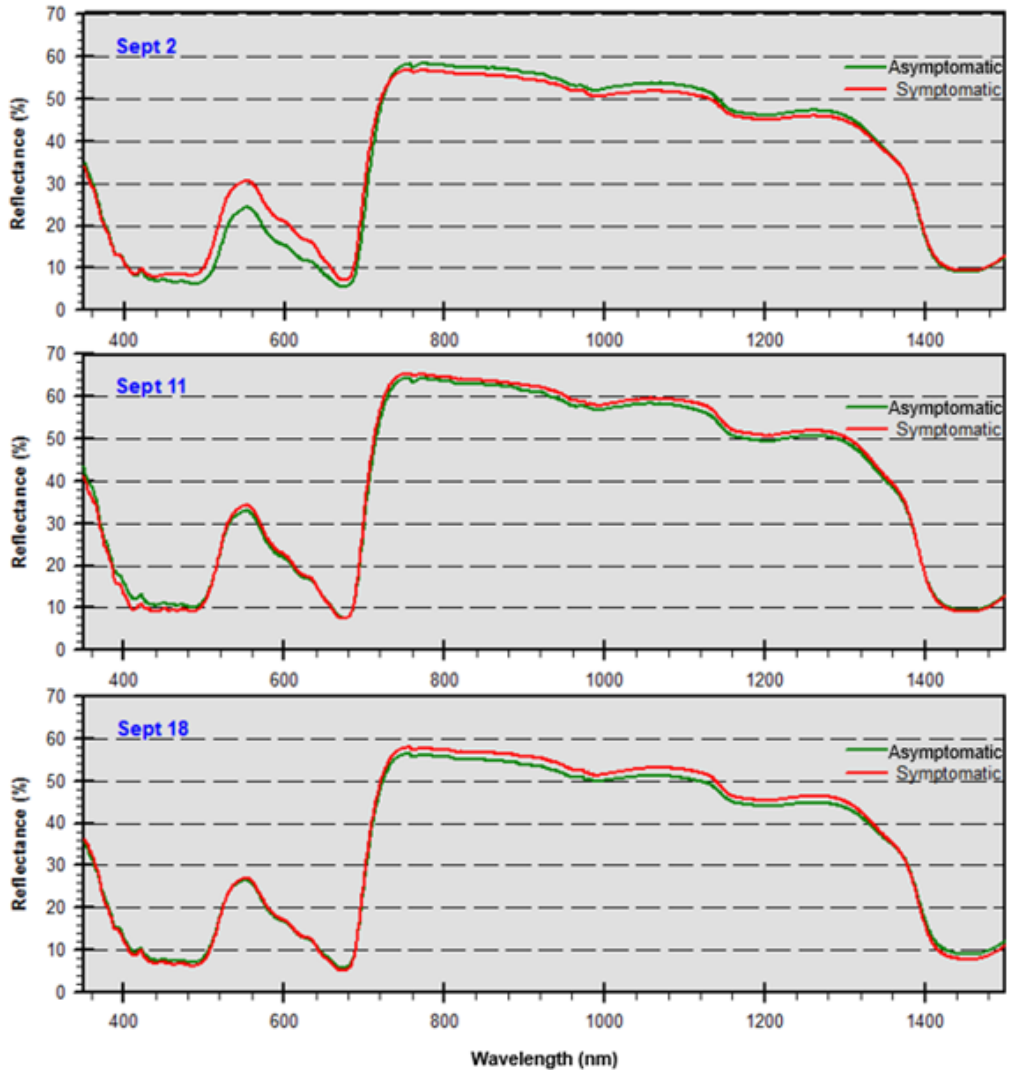

Figure 7. Mean spectral profiles of the asymptomatic and symptomatic groups for all three observation dates of the 2018 Granville wilt study conducted near Kenbridge, VA.

for future applications in flue-cured tobacco disease management.

References

1. M. Daub, G. Lucas and H. Shew, *Compendium of Tobacco Diseases*. The American Phytopathological Society, St Paul, Minnesota (1991).
2. A. Sahu and H. Dante, "Non-destructive rapid quality control method for tobacco grading using visible near-infrared hyperspectral imaging", *Proc. SPIE 10656, Image Sensing Technologies: Materials, Devices, Systems, and Applications V*, 1065603 (2018). https://doi.org/10.1117/12.2305091
3. F. Jia, G. Liu, D. Liu, Y. Zhang, W. Fan and X. Xing, "Comparison of different methods for estimating nitrogen concentration in flue-cured tobacco leaves based on hyperspectral reflectance", *Field Crops Res.* **150,** 108–114 (2013). https://doi.org/10.1016/j.fcr.2013.06.009
4. F. Jia, G. Liu, S. Ding, Y. Yang, Y. Fu and Z. Wang, "Using leaf spectral reflectance to monitor the effects of shading on nicotine content in tobacco leaves", *Ind. Crop. Prod.* **51,** 444 (2013). https://doi.org/10.1016/j.indcrop.2013.09.027
5. P. Mishra, S. Lohumi, H.A. Khan and A. Nordon, "Close-range hyperspectral imaging of whole plants for digital phenotyping: recent applications and illumination correction approaches", *Comput. Electron. Agr.* **178,** 105780 (2020). https://doi.org/10.1016/j.compag.2020.105780
6. H. Zhu, B. Chu, C. Zhang, F. Liu, L. Jiang and Y. He, "Hyperspectral imaging for presymptomatic

detection of tobacco disease with successive projections algorithm and machine-learning classifiers", *Sci. Rep.* **7,** 4125 (2017). https://doi.org/10.1038/s41598-017-04501-2

7. P. Moghadam, D. Ward, E. Goan, S. Jayawardena, P. Sikka and E. Hernandez, "Plant disease detection using hyperspectral imaging", in *2017 International Conference on Digital Image Computing: Techniques and Applications (DICTA), Sydney, NSW, 2017*, pp. 1–8 (2017). https://doi.org/10.1109/DICTA.2017.8227476
8. T. Chen, J. Zhang, Y. Chen, S. Wan and L. Zhang, "Detection of peanut leaf spots disease using canopy hyperspectral reflectance", *Comput. Electron. Agr.* **156,** 677–683 (2019). https://doi.org/10.1016/j.compag.2018.12.036
9. J. Lu, M. Zhou, Y. Gao and H. Jiang, "Using hyperspectral imaging to discriminate yellow leaf curl disease in tomato leaves", *Precis. Agric.* **3,** 379–394 (2018). https://doi.org/10.1007/s11119-017-9524-7
10. K. Nagasubramanian, S. Jones, S. Sarkar, A.K. Singh, A. Singh and B. Ganapathysubramanian, "Hyperspectral band selection using genetic algorithm and support vector machines for early identification of charcoal rot disease in soybean stems", *Plant Meth.* **14(1),** 1–13 (2018). https://doi.org/10.1186/s13007-018-0349-9
11. A. Mahlein, E. Oerke, U. Steiner and H. Dehne, "Recent advances in sensing plant diseases for precision crop protection", *Eur. J. Plant Pathol.* **1,** 197–209 (2012). https://doi.org/10.1007/s10658-011-9878-z
12. P. Mishra, G. Polder and N. Vilfan, "Close range spectral imaging for disease detection in plants using autonomous platforms: a review on recent studies", *Agric. Robot.* **1,** 43–48 (2020). https://doi.org/10.1007/s43154-020-00004-7
13. S. Prasad and L. Bruce, "Limitations of principal components analysis for hyperspectral target recognition", *IEEE Geosci. Remote Sens. Lett.* **5(4),** 625–629 (2008). https://doi.org/10.1109/LGRS.2008.2001282
14. A. Sahu, H. Dante, E. Haase and J.W. Morris, "Hyperspectral imaging using CCD imager and broadband energy source for agricultural grading: implementation", *Proc. SPIE 10754, Wide Bandgap Power and Energy Devices and Applications III*, 107540G (2019). https://doi.org/10.1117/12.2323721